Appl. Phys. B 76, 417–421 (2003)
DOI: 10.1007/s00340-003-1094-x

Applied Physics B
Lasers and Optics

A. SHUMELYUK[1]
D. BARILOV[1]
S. ODOULOV[1,✉]
E. KRÄTZIG[2]

Anisotropy of the dielectric permittivity of $Sn_2P_2S_6$ measured with light-induced grating techniques

[1] Institute of Physics, National Academy of Sciences, 03650 Kiev, Ukraine
[2] Fachbereich Physik, Universität Osnabrück, 49069 Osnabrück, Germany

Received: 2 December 2002
Published online: 26 March 2003 •

ABSTRACT We apply, for the first time to our knowledge, photorefractive grating spectroscopy to obtain not-yet-known data on the anisotropy of the dielectric permittivity of $Sn_2P_2S_6$. Two independent techniques are used, one based on measurements of the amplitude of the space-charge field grating as a function of grating spacing and the other based on measurements of the grating decay time, also as a function of grating spacing. Both techniques provide close values for the anisotropy, which appears to be well pronounced, a ratio $\varepsilon_{xx}/\varepsilon_{zz} \approx 4$ is revealed for two of the three independent components of the dielectric tensor. Our data also allow us to conclude that the charge mobility is nearly isotropic in the same plane, $\mu_{xx}/\mu_{zz} \approx 1$.

PACS 42.65.Hw; 42.70.Nq; 77.22.Ch

1 Introduction

Tin hypothiodiphosphate ($Sn_2P_2S_6$) is a low-symmetry (m) ferroelectric material transparent in the red and near-infrared regions of the spectrum [1, 2]. It features a rather strong electro-optic effect (one of the ten independent components of the electro-optic tensor reaches a value of 130 pm/V [3, 4]), good pyroelectric and piezoelectric properties [5] and can be used for second-harmonic generation [6]. It is attractive also as a photorefractive crystal, with a rather fast temporal response (in the millisecond range for conventional cw lasers) and a sufficiently high gain factor (up to $15\,\mathrm{cm}^{-1}$ for 1-μm [4, 7] and up to $40\,\mathrm{cm}^{-1}$ for 0.63-μm [8] wavelengths). In spite of the large amount of information on this crystal, collected during the thirty years after it was first synthesized, some data on its fundamental constants are still unknown; for some other constants there is a large discrepancy between data obtained with different techniques. One can find, for example, for the low-frequency dielectric constant a value $\varepsilon = 3500$ in the Landolt–Börnstein sourcebook [9] and a more than one-order-of-magnitude smaller value in the original publication [10]. There are also no reliable data to our knowledge on the anisotropy of the dielectric permittivity.

✉ Fax: +380-44/265-2359, E-mail: odoulov@iop.kiev.ua

We extracted the data on the dielectric permittivity from measurements of the dynamics of the space-charge field gratings that can be induced in the crystal by laser light via the photorefractive effect (see, for example, [11]). An advantage of any grating technique is that it allows the study of tensor properties simply by changing the orientation of the recording light waves in a way to align the grating vector $\boldsymbol{K} = \boldsymbol{k}_1 - \boldsymbol{k}_2$ along the crystallographic axes [12]. (Here $\boldsymbol{k}_1$ and $\boldsymbol{k}_2$ are the wave vectors of the recording waves.) We profit from this possibility for studying the anisotropy of the low-frequency dielectric constant ε.

The ultimate amplitude of the space-charge field grating is limited by the finite trap density and the dielectric constant of the crystal. By comparing these amplitudes for gratings aligned along two crystallographic axes we can obtain the ratio of the dielectric constants, assuming the traps are distributed inside the crystal homogeneously.

The decay of the space-charge gratings occurs via the usual Maxwell dielectric relaxation, i.e. because of the finite conductivity σ. The characteristic decay time τ depends therefore on the dielectric permittivity, $\tau \propto \varepsilon\varepsilon_0/\sigma$. This provides an independent tool for the evaluation of ε.

After recalling some basic data on photorefractive grating recording and presenting the main theoretical expressions that will allow us to extract the data on ε, the description of the experiment is given and finally the data obtained with the different techniques are compared.

2 Physical background

If photoconducting crystals (like $BaTiO_3$, $Sr_xBa_{1-x}NbO_3$, $LiNbO_3$ and some others) are illuminated with two coherent light waves (see Fig. 1a,b), the density of free carriers photoexcited from the deep centers is spatially modulated. The gradients in the carrier density give rise to diffusion currents, which tend to wash out this inhomogeneous distribution; as a consequence, a part of the carriers appears in the dark region of the light fringes, where the ionized centers trap them. In such a way, a periodic space-charge distribution is formed in the bulk of the crystal and the static electric field of this space charge modifies the refractive index of the crystal via the electro-optic effect. This type of optical non-linearity is traditionally called the diffusion-driven photorefractive effect [11].

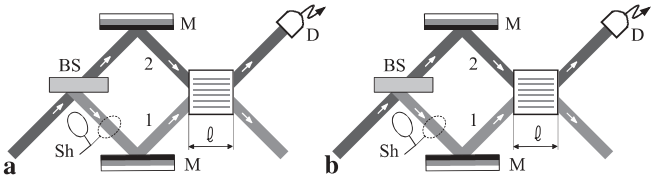

FIGURE 1 Schematic representation of the experimental geometry to study the dynamics of recording in transmission (**a**)and reflection (**b**) geometry. SPS is the sample; D, the detector; Sh, the shutter; M, mirrors; and BS, the beam splitter

In crystals lacking a symmetry center, the developing refractive index grating appears to be $\pi/2$-shifted with respect to the light fringes; this results in a unidirectional intensity transfer from the one of the two recording waves to the other because of self-diffraction from the grating. The measure of such a beam coupling is the gain factor Γ, which is introduced as:

$$\Gamma = \frac{1}{\ell} \ln \left[\frac{I_1(\ell)}{I_1(0)} \frac{I_2(0)}{I_2(\ell)} \right], \tag{1}$$

where $I_{1,2}(0)$ and $I_{1,2}(\ell)$ are the intensities of the two recording waves 1 and 2 at the input face ($z = 0$) and at the output face ($z = \ell$) of the sample.

According to theory [13], the gain factor is proportional to a light-induced variation of the refraction index, i.e. directly proportional to the space-charge electric field. The final expression for Γ reads:

$$\Gamma = \frac{4\pi^2 n^3 r_{\text{eff}}}{\Lambda \lambda \cos\theta} \frac{k_B T}{e} \frac{1}{1 + (\ell_s/\Lambda)^2}, \tag{2}$$

with the light wavelength λ in vacuum, the refraction index n, the effective electro-optic coefficient r_{eff}, the Boltzmann constant k_B, the absolute temperature T, the electron charge e, the angle 2θ between the two recording waves (inside the crystal), the grating spacing $\Lambda = \lambda/2n \sin\theta$, and the Debye screening length

$$\ell_s = \sqrt{\frac{\varepsilon\varepsilon_0 k_B T}{e N_{\text{eff}}}}, \tag{3}$$

N_{eff} being the effective trap density.

As one can see from (2), the gain factor reaches its maximum value at a grating spacing Λ equal to the Debye screening length ℓ_s. This allows for experimental determination of ℓ_s which depends, as it follows from (3), on the dielectric permittivity ε.

The space-charge grating can be erased by uniform illumination of the sample. A light wave with intensity I excites free carriers and increases the conductivity. The photoconductivity of the sample is $\sigma = \kappa I$, with κ being the specific photoconductivity. For any of the two types of carriers (electrons or holes), the theory [14] predicts a single-exponential decay of the space-charge grating with its own characteristic time τ:

$$\frac{1}{\tau I} = \frac{\kappa}{\varepsilon\varepsilon_0} \frac{1 + (\ell_s/\Lambda)^2}{1 + (\ell_D/\Lambda)^2}. \tag{4}$$

Here the diffusion length is given by the expression:

$$\ell_D = \sqrt{D\tau_{fc}}, \tag{5}$$

where τ_{fc} is the free carrier lifetime and D is the diffusivity, related to the charge mobility μ via:

$$D = \mu \frac{k_B T}{e}. \tag{6}$$

It follows from (4) that the dielectric permittivity enters twice in (4), in the numerator (via ℓ_s, see (3)) and also directly in the denominator. By changing the angle θ between the recording waves it is possible to vary the grating fringe spacing Λ in a rather wide range and to meet either the condition $(\ell_s/\Lambda) \gg 1$ or $(\ell_s/\Lambda) \ll 1$. This offers several possibilities for extracting the data on ε from the angular dependencies of the decay rate, as is discussed later.

It should be noted that some experimental data [7] suggest a charge-hopping type of photoconductivity [15] for $Sn_2P_2S_6$. It has been shown, however, that all equations listed above are applicable to the space-charge formation and decay via "hopping" transport as well as for diffusion-driven transport [16]. The meaning of some quantities like the charge mobility or the diffusivity becomes slightly modified for the hopping process, while the meaning of such a fundamental constant like the dielectric permittivity remains the same.

$Sn_2P_2S_6$ is known to possess two types of movable charge carriers, with a dielectric relaxation time that differs by several orders of magnitude for the two subsystems [7]. This huge difference allows for easy separation of the effects related to each type of carrier and for receiving reliable data on the decay time of each subsystem. This all justifies the use of the equations presented above for the comparison with the experimental results on $Sn_2P_2S_6$. All measurements described in what follows have been carried out for the fast photorefractive grating that is formed in $Sn_2P_2S_6$ by photoexcited holes [17].

3 Experimental

The crystals of nominally undoped tin hypothiodiphosphate studied were grown via gas transport reaction [18] in the Institute of Physics and Chemistry of the Solid State, University of Uzhgorod, Ukraine. The sample cut along the crystallographic axes measured $9 \times 9 \times 4.5\,\text{mm}^3$; it had optically finished faces normal to the $\boldsymbol{X}$- and $\boldsymbol{Z}$-directions. The sample K3 belonged to the type-I crystals [4, 19], with a pronounced contribution of secondary carriers to the grating formation. It was poled by application of an external field of about 1 kV/cm when the sample was heated to 90 °C.

A helium–neon laser with a 40-mW TEM_{00} output beam was used as a light source. Two light beams impinged upon the sample, either from the same face (transmission-grating geometry) or from two opposite faces (reflection-grating geometry). The orientation of the grating vector $\boldsymbol{K}$ remained the same for one set of measurements in transmission and reflection geometries; for the second set of measurements, $\boldsymbol{K}$ was aligned along the other crystallographic axis and also remained the same for transmission and reflection geometries. The polarization of the recording waves was normal to the plane of drawing in Fig. 1, i.e. the electric field vector of the light waves was always parallel to the $\boldsymbol{Y}$ axis. Unexpanded laser beams were used with a beam diameter of 1.4 mm at a 1/e intensity level from the maximum and the total intensity at the input face was about $3\,\text{W/cm}^2$.

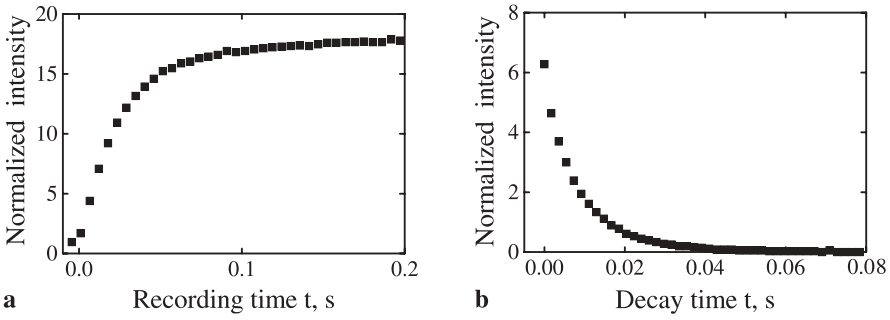

FIGURE 2 Temporal evolution of the intensity of the transmitted light wave 1, measured during grating recording (**a**) and temporal evolution of the intensity of the light wave diffracted in the direction of wave 1 (**b**) when the input wave 1 is stopped by a shutter

Figure 2a and b shows a typical temporal evolution of the intensity of one of the two recording beams during recording and optical erasure, respectively. At first two beams exposed the sample and the intensity of one beam increased until saturation because of beam coupling. Further exposure of the sample to the fringe pattern would result in a decrease of the light intensity because of formation of an out-of-phase grating by free carriers of opposite sign [7]. We stopped the exposure when the intensity reached its maximum value. The data on beam coupling presented in Fig. 2a were sufficient to calculate the gain factor if the initial intensity of the amplified wave 1 was much smaller than that of the second recording wave 2 (see (1)).

After the maximum intensity of the transmitted weak wave 1 was reached, the input wave was stopped with a shutter placed in front of the sample. The detector then measured the decay of the intensity of the beam diffracted from the grating (Fig. 2b). By fitting this curve to an exponential function we obtained the decay time of the grating efficiency, which was half as large as the space-charge decay time that we were searching for.

In a next step, measurements of the gain factor and of the characteristic decay rates were performed for different angles of incidence of the recording waves to obtain the dependencies $\Gamma = \Gamma(\Lambda)$ and $\tau^{-1} = \tau^{-1}(\Lambda)$. This was done for two orientations of the grating vector $\boldsymbol{K}$, parallel to crystallographic axes $\boldsymbol{K} \parallel \boldsymbol{X}$ and $\boldsymbol{K} \parallel \boldsymbol{Z}$.

Figure 3 represents the results of gain factor measurements. Empty dots and squares give the values measured in transmission grating geometry (Fig. 1a), while filled dots and squares correspond to recording with counterpropagating waves (reflection grating geometry, Fig. 1b). The dots represent the values measured with $\boldsymbol{K} \parallel \boldsymbol{X}$ while data for $\boldsymbol{K} \parallel \boldsymbol{Z}$ are shown by squares. It should be mentioned that with the recording beam diameter $d = 1.4$ mm and the sample thickness

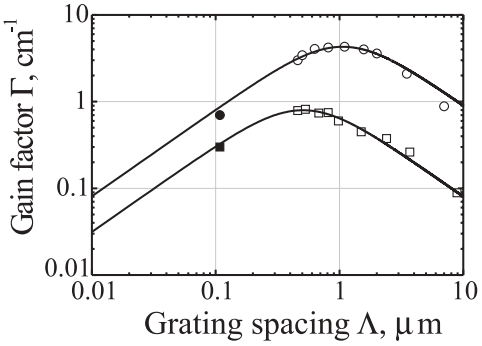

FIGURE 3 Grating spacing dependencies of the gain factor for a grating vector aligned along the sample's $\boldsymbol{Z}$ axis (*squares*) and along the $\boldsymbol{X}$ axis (*dots*). The recording light is polarized parallel to the *y* axis. *Open dots* and *squares* represent measurements with copropagating laser beams, while *filled dots* and *squares* correspond to a counterpropagating beam geometry. *Solid lines* are best fits by the calculated dependence (2)

$\ell = 9$ mm, the beams were overlapping incompletely inside the sample and the effective interaction length ℓ_{eff} became smaller than the sample thickness ℓ (see, for example, [7]):

$$\ell_{\text{eff}} = \ell \left(1 - \frac{\pi \ell \sin\theta}{4d}\right). \tag{7}$$

This was taken into account when calculating the values of the gain factor plotted in Fig. 3. The solid lines are fits of the calculated dependence given by (2).

The data on the grating decay rate presented in Fig. 4 are normalized to the light intensity; in fact each value of $(1/\tau I)$ was extracted from the intensity dependence of the decay time $\tau = \tau(I)$ measured for a particular angle between the recording waves. The plot of $(1/\tau I)$ versus the squared reciprocal grating spacing simplifies the comparison with (4). The meaning of the open and filled dots and squares is the same as that

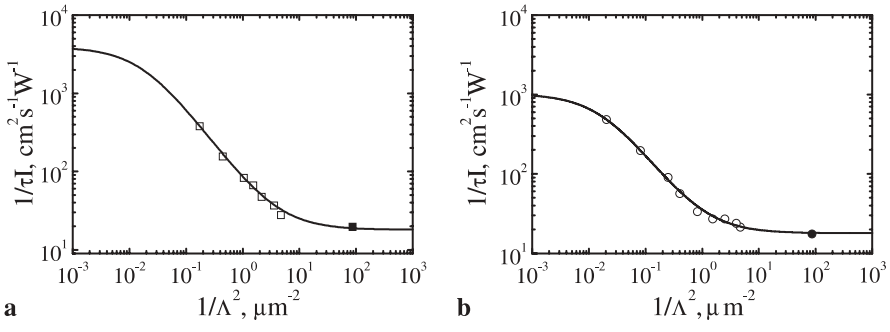

FIGURE 4 Reciprocal decay time versus squared reciprocal grating spacing for a grating vector aligned along the samples $\boldsymbol{Z}$ axis (**a**) and along the $\boldsymbol{X}$ axis (**b**). *Open dots* and *squares* represent measurements with copropagating laser beams while *filled dots* and *squares* correspond to a counterpropagating beam geometry. *Solid lines* are best fits of the calculated dependence (4)

for Fig. 3. The solid lines are fits of the calculated dependencies given by (4). In these measurements, the changes in the light intensity inside the sample, which were due to a different Fresnel reflectivity at different angles and the beam cross section varying with the angle, were neglected. With the polarization used and within the experimental range of angles, these changes were below 15%.

4 Evaluation of the transport lengths and the anisotropy of permittivity

The experimental data presented in Figs. 3 and 4 allowed us to extract the characteristic transport lengths, the Debye screening length ℓ_s and the diffusion length ℓ_D. The first of these two lengths is determined from the position of the maximum of the $\Gamma = \Gamma(\Lambda)$ dependencies (Fig. 3). We get $\ell_{sx} \approx 1.0\,\mu$m for the x-direction while only $\ell_{sz} \approx 0.52\,\mu$m for the $\boldsymbol{Z}$-direction (extra subscripts for ℓ_s, z and x, respectively.)

The values of the gain factor measured in reflection geometry were quite close to the $\Gamma = \Gamma(\Lambda)$ dependencies shown by solid lines and obtained by the least square fit technique. An important question is: do we have to keep reflection-hologram data or it is possible to omit these and to obtain, nevertheless, a reliable fit and the same parameters? To answer this question we compare the values of the screening length extracted from the whole set of measurements including data for reflection geometry with that extracted from data on transmission geometry only. The results are as follows: The fit of all experimental data by (8) provides $\ell_{sz} = 0.50 \pm 0.03\,\mu$m for $\boldsymbol{K} \parallel \boldsymbol{Z}$ while the fit to data for transmission geometry yields $\ell_{sz} = 0.52 \pm 0.03\,\mu$m. A similar comparison for $\boldsymbol{K} \parallel \boldsymbol{X}$ gives for the whole set of data $\ell_{sx} = 1.0 \pm 0.04\,\mu$m and $\ell_{sx} = 0.99 \pm 0.04\,\mu$m for transmission geometry only. It is clear from this comparison that the data for reflection geometry are good for verifying the dependence of (2) (or (8)), but they are not so critical for extracting ℓ_s.

The data on the gain factor (Fig. 3) are also useful for the evaluation of the electro-optic tensor components. It is convenient to plot the data of Fig. 3 in special coordinates, $(1/\Gamma\Lambda)$ versus $(1/\Lambda^2)$ in Fig. 5, as proposed in [20] to obtain a linear dependence:

$$\frac{1}{\Gamma\Lambda} = \frac{\lambda\cos\theta}{4\pi^2 n^3 \xi r_{\text{eff}}} \frac{e}{k_B T}\left[1 + \left(\frac{\ell_s}{\Lambda}\right)^2\right]. \tag{8}$$

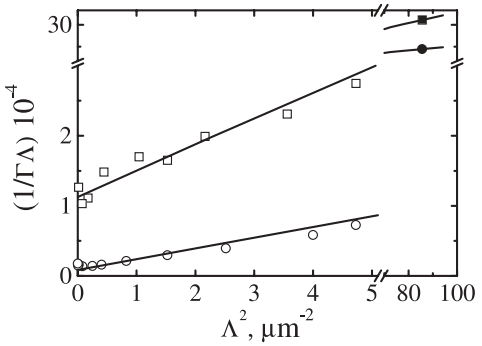

FIGURE 5 Dependencies $1/\Gamma\Lambda = f\left(1/\Lambda^2\right)$ for the evaluation of crystal parameters (see text) re-plotted from the data of Fig. 3

From the intersection point of this straight line with the ordinate, the product of the two first factors on the right-hand side of (8) can be evaluated with only one unknown parameter, which is ξr_{eff}, while from the slope of this line we get an estimate for ℓ_s [20]. A factor $0 < \xi < 1$ accounts for a possibly incomplete poling of the ferroelectric sample, i.e. for the presence of domains with an opposite orientation of spontaneous polarization. The values of ξr_{eff} that come out of these fits are $\xi r_{221} \approx 17$ pm/V and $\xi r_{223} \approx 2$ pm/V. These values should be regarded, however, as a lower limit for r_{221} and r_{223} because the amount of domains with the opposite direction of spontaneous polarization in the sample is unknown.

The next step is to process the data of Fig. 4 by imposing the already known values of ℓ_{sx} and ℓ_{sz}. By fitting these data by (4) we extracted the diffusion length for different crystallographic directions, $\ell_{Dx} \approx 7.5 \pm 0.2\,\mu$m and $\ell_{Dz} \approx 7.8 \pm 1.0\,\mu$m. Taking into account the definition of the diffusion length (5) we conclude that the anisotropy of the charge mobility for charges involved in the formation of the fast grating in $Sn_2P_2S_6$ is rather small in the $\boldsymbol{X}0\boldsymbol{Z}$ plane.

In addition, it is possible to evaluate the first factor in the right-hand side of (4). The fit yields $(\kappa_{zz}/\varepsilon_{zz}\varepsilon_0) \approx 4200\,\text{cm}^2/\text{W s}$ and $(\kappa_{xx}/\varepsilon_{xx}\varepsilon_0) \approx 1000\,\text{cm}^2/\text{W s}$. With a small difference in the charge mobilities, the photoconductivity is nearly isotropic in the $\boldsymbol{X}0\boldsymbol{Z}$ plane, too, $\kappa_{xx} \approx \kappa_{zz}$ and the anisotropy of $(\kappa/\varepsilon\varepsilon_0)$ can be attributed mainly to the anisotropy of the dielectric permittivity.

To obtain an estimate for the absolute value of ε one should know either the effective trap density N_{eff} or the specific photoconductivity κ. Both quantities need to be evaluated independently directly from electrical measurements, which is out of the scope of the present paper. From the optical measurements we performed, we can extract, however, the data on the anisotropy of the dielectric permittivity, i.e. the ratio $\varepsilon_{xx}/\varepsilon_{zz}$. This quantity can be extracted from the ratio of the Debye screening lengths:

$$\frac{\varepsilon_{xx}}{\varepsilon_{zz}} = \left(\frac{\ell_{sx}}{\ell_{sz}}\right)^2 \approx 3.7 \pm 0.7\,, \tag{9}$$

and also from the ratio of the first factors in the right-hand side of (4):

$$\frac{\varepsilon_{xx}}{\varepsilon_{zz}} \approx 3.9 \pm 0.2\,. \tag{10}$$

The reasonable agreement of the two estimates within the given range of the experimental accuracy is obvious.

We need to remind ourselves once more that one must know the anisotropy of the specific photoconductivity κ to evaluate $\frac{\varepsilon_{xx}}{\varepsilon_{zz}}$ using the second technique. It is important to underline that for the polarization used (normal to $\boldsymbol{X}0\boldsymbol{Z}$ plane) the absorptivity does not depend on the orientation of the light beam in the $\boldsymbol{X}0\boldsymbol{Z}$ plane for crystals with the symmetry m. With a rather small (if any) anisotropy of the mobility, the photoconductivity κ is nearly isotropic too.

An independent check of the validity of the second proposed technique is as follows: In the limit of small grating spacings, $\Lambda \to 0$, i.e. $(\ell_s/\Lambda) \gg 1$, one can neglect the unity in the numerator as well as in the denominator of the second

factor in the right-hand side of (4) and arrive at:

$$\frac{1}{\tau I} = \frac{\ell_s^2}{\varepsilon\varepsilon_0}\frac{\kappa}{\ell_D^2}. \tag{11}$$

From the definition of the Debye screening length (3) it is clear that the first factor in (11) $\left(\ell_s^2/\varepsilon\varepsilon_0\right)$ does not depend on the dielectric permittivity. It is easy to show also that the second factor $\left(\kappa/\ell_D^2\right)$ does not depend on the possible anisotropy of free carrier mobility. From symmetry considerations it follows that the absorption constant for light polarised along the y axis is isotropic in the $\boldsymbol{X}0\boldsymbol{Z}$ plane. Thus the right-hand side of (11) contains no anisotropic quantities and should therefore be the same for an arbitrary orientation of the grating vector.

For the small spacing limit, our fits give the same values $(1/\tau I) \approx 18.0\,\mathrm{cm}^2/\mathrm{W\,s}$ measured along the $\boldsymbol{Z}$ axis and along the $\boldsymbol{X}$ axis. Taking into account that $(1/\tau I)$ varies more than two orders of magnitude within the whole range of grating spacing variation, this coincidence can hardly be accidental and is in agreement with our expectations.

In crystals belonging to the symmetry class m, the relation $r_{112} = r_{222} = r_{332} \equiv 0$ holds for the electro-optic coefficients, and self-diffraction from space-charge gratings with the grating vector aligned along the y axis is impossible. This is the reason why we report on the anisotropy of the $Sn_2P_2S_6$ parameters in the $\boldsymbol{X}0\boldsymbol{Z}$ plane only. In principle, the non-vanishing electro-optic coefficients r_{232} and r_{212} allow for anisotropic diffraction with the polarization of the diffracted wave orthogonal to the polarization of the readout wave. To observe this type of diffraction one should ensure, however, appropriate Bragg angles that do not coincide with the recording angles.

5 Conclusions

By using all-optical techniques based on the study of the dynamics of grating recording and erasure, we discovered a strong anisotropy in the dielectric permittivity in tin hypothiodiphosphate ($Sn_2P_2S_6$) at ambient temperature, $\varepsilon_{xx}/\varepsilon_{zz} \approx 4$. It follows from our measurements that the photoexcited hole mobility is nearly insensitive to direction in the same plane, $\mu_{xx}/\mu_{zz} \approx 1$.

The grating spectroscopy techniques also allow the evaluation of the anisotropy of the electro-optic properties [4]. Our estimates give rather small values for $\xi r_{221} \approx 17\,\mathrm{pm/V}$ and $\xi r_{223} \approx 2\,\mathrm{pm/V}$. It should be underlined, however, that these relatively weak components were selected deliberately for the measurements of the ε-anisotropy: firstly, we were well within the undepleted pump approximation when measuring gain factors; secondly, just these components were involved in recording of both transmission and reflection gratings; and last, but not least, there was no absorption anisotropy for the chosen geometry and light polarization.

ACKNOWLEDGEMENTS The support of the Alexander von Humboldt Foundation is gratefully acknowledged. We are grateful to Dr. A. Grabar for the $Sn_2P_2S_6$ sample and for fruitful discussions.

NOTE ADDED IN PROOF Our attention was drawn recently to publication V.M. Kedyulich, A.G. Slivka, E.I. Gerzanich, P.P. Guranich, V.S. Shusta, and P.M. Lucach, Uzhgorod University Bulletin, Phys. Ser. **5** 30–32 (1999), in which the dielectric constants of $Sn_2P_2S_6$ have been measured electrically. The reported anisotropy $\varepsilon_{xx}/\varepsilon_{zz} \simeq 4$ at ambient temperature is in good agreement with the results presented in our paper.

REFERENCES

1 G. Dittmar, H. Schaefer: Z. Naturforschung **29b**, 312 (1974)
2 M.I. Gurzan, A.P. Buturlakin, V.S. Gerasimenko, N.F. Korda, V.Y. Slivka: Sov. Phys. Solid State **19**, 1794 (1977)
3 R.O. Vlokh, Y.M. Vysochanski, A.A. Grabar, A.V. Kityk, V.Y. Slivka: Bull. USSR Acad. Sci. Inorg. Mater. **27**, 570 (1991)
4 A. Shumelyuk, S. Odoulov, D. Kip, E. Krätzig: Appl. Phys. B **72**, 707 (2001)
5 S.L. Bravina, L.S. Kremenchugskii, M.D. Kladkievich, N.V. Morozovskii, V.B. Samoilov, M.M. Maior, M.I. Gurzan, Y.M. Vysochanski, V.Y. Slivka: Bull. USSR Acad. Sci. Inorg. Mater. **23**, 657 (1987)
6 A.V. Gomonnaj, A.A. Grabar, Y.M. Vysochanski, A.D. Belyaev, V.F. Machulin, M.I. Gurzan, V.Y. Slivka: Sov. Phys. Solid State **23**, 2093 (1981)
7 S. Odoulov, A. Shumelyuk, U. Hellwig, R. Rupp, A. Grabar, I. Stoyka: J. Opt. Soc. Am. B **13**, 2352 (1996)
8 A.A. Grabar, I.V. Kedyk, M.I. Gurzan, I. Stoyka, A.A. Molnar, Y.M. Vysochanski: Opt. Commun. **188**, 187 (2001)
9 K.H. Hellwege (Ed.): *Landolt–Börnstein Numerical Data and Functional Relationships in Science and Technology, New Series, Gruppe III*, Vol. 16/B (Springer-Verlag, Berlin 1982) p. 290 Fig. 1623; p. 693. Ref. 77B19
10 A.A. Volkov, G.V. Kozlov, N.I. Afanasieva, Y.M. Vysochansky, A.A. Grabar, V.Y. Slivka: Sov. Phys. Solid State **25**, 1482 (1983)
11 L. Solymar, D.J. Webb, A. Grunnet-Jepsen: *The Physics and Applications of Photorefractive Materials* (Clarendon, Oxford 1996)
12 H.J. Eichler, P. Guenter, D.W. Pohl: *Laser-Induced Dynamic Gratings* (Springer-Verlag, Berlin 1986)
13 N.V. Kukhtarev, V.B. Markov, S.G. Odoulov, M.S. Soskin, V.L. Vinetskiy: Ferroelectrics **22**, 949 (1979)
14 F.P. Strohkendl, J.M.C. Jonathan, R.W. Hellwarth: Opt. Lett. **11**, 312 (1986)
15 J. Feinberg, D. Heiman, A.R. Tanguay, R.W. Hellwarth: J. Appl. Phys. **51**, 1297 (1980)
16 R.A. Mullen: In *Photorefractive Materials and their Applications I, Springer Topics in Applied Physics*, Vol. 61, ed. by P. Günter, J.P. Huignard (Springer-Verlag, Berlin 1988)
17 I. Seres, S. Stepanov, S. Mansurova, A.A. Grabar: J. Opt. Soc. Am. B **17**, 1986 (2000)
18 C.D. Carpenter, R. Nitche: Mater. Res. Bull. **9**, 401 (1974)
19 A. Shumelyuk, S. Odoulov, G. Brost, U. Hellwig, Y. Hu, E. Kräetzig: 'Ti–Sapphire Laser Beam Coupling in $Sn_2P_2S_6$'. In *CLEO'98 Technical Digest* (Opt. Soc. of Am., San Francisco 1998) pp. 171–172
20 M.B. Klein, G.C. Valley: J. Appl. Phys. **57**, 4109 (1997)